Microsystems and mechanics

Alberto Corigliano*, Raffaele Ardito, Claudia Comi, Attilio Frangi, Aldo Ghisi, Stefano Mariani

Department of Structural Engineering, Politecnico di Milano, piazza Leonardo da Vinci 32, Milano 20133, Italy

1. Introduction

Microsystems (or Micro electro mechanical systems, MEMS) are complex devices, produced with technologies similar to the ones used for integrated circuits, in which dimensions can reduce up to fractions of micrometers [1–4]. Microsystems technology can nowadays be used to produce highly miniaturized sensors such as accelerometers and gyroscopes, or actuators which in turn can be used to create e.g. micro-pumps or energy harvesting devices.

The great versatility and the reduced unit cost have been the basic ingredients for their large diffusion; microsystems are in fact nowadays complex products of modern engineering which find a large number of applications in various fields such as consumer and automotive engineering, structural monitoring, biomedical engineering.

* Corresponding author. Tel.: +39 0223994244; fax.: +39 0223994220.
E-mail address: alberto.corigliano@polimi.it.

Mechanical issues, and particularly mechanical reliability, are extremely important in all the phases of MEMS design and in the development of relevant production technology: proper design and fabrication of micro-devices must ensure the perfect functioning both in standard exercise conditions and in extreme situations (e.g. accidental drop, mechanical and electrical shock, harsh environment, etc.).

The purpose of this paper is to describe some aspects of the complexity of microsystems from a mechanical perspective with particular reference to dissipative phenomena and mechanical reliability problems. The focus is on specific issues which have been studied by the group in the last nine years in strict collaboration with STMicroelectronics, which is one of the major microsystem manufacturer, and with particular reference to solid mechanics. In Sects. 2 and 3, starting from a very brief introduction to fabrication technologies and from the analysis of a uniaxial resonant micro-accelerometer taken as a meaningful example, the major mechanical features and challenges related to microsytems mechanics are highlighted. The subsequent Sections are dedicated to a brief presentation of four major issues concerning microsystem mechanics: the dissipative phenomena which govern the damping of vibrating devices (Sect. 4), the mechanical characterization of materials at the scale of microsystems (Sect. 5), the response to accidental impacts (Sect. 6), the study of spontaneous adhesion or stiction (Sect. 7). Closing remarks and perspectives are included in Sect. 8.

2. Fabrication process

Microsystems are produced with fabrication technologies which originate from modifications of planar lithographic technologies used since many years for the production of integrated circuits (IC), the main modification of these processes being the introduction of movable parts (see [4]). The examples shown in this paper refer to devices produced by STMicroelectronics with the surface micro-machining process (thick epipoly layer for microactuators and accelerometers) ThELMA^{TM} which has been developed by STMicroelectronics to realize in-silicon inertial sensors and actuators (see also [5] for further details). This process is here briefly described in order to give an idea of how microsystems are realized and of the possibilities and constraints that a microsystem designer can face.

The Thelma process permits the realization of suspended structures anchored to the substrate through very compliant parts (springs) and thus capable of moving with respect to the underlying silicon substrate; it consists of the phases described hereafter and illustrated schematically in Fig. 1.

(1) Substrate thermal oxidation. The silicon substrate is covered by a 2.5 μm thick layer of permanent oxide obtained with a thermal treatment at 1 100 $^{\circ}$C.
(2) Deposition and patterning of horizontal interconnections. The first polysilicon layer is deposited above the thermal oxide; this layer (poly1) is used to define the buried runners which are used to bring potential and capacitance signals outside the device and it can also be used as structural layer in thin polysilicon devices.
(3) Deposition and patterning of a sacrificial layer. A 1.6 μm thick oxide layer is deposited by means of a plasma enhanced chemical vapour deposition (PECVD) process. This layer, together with the thermal oxide layer, forms a 4.1 μm thick layer which separates the moving part from the substrate and which can be considered analogous with the sacrificial layer in a surface micromachining process.
(4) Epitaxial growth of the structural layer (thick polysilicon). The polysilicon is made grow in the reactors, thus reaching a thickness of 15 μm.
(5) Structural layer patterning by trench etch. The parts of the mobile structure are obtained by deep trench etch which reaches the oxide layer.
(6) Sacrificial oxide removal and contact metallization deposition. The sacrificial oxide layer is removed with a chemical reaction; in order to avoid stiction (see Sect. 7) due to attractive capillary reactions, this is done in rigorously dry conditions. The contact metallization is deposited; it will be used to make the wire-bonding between the device and the metallic frame.

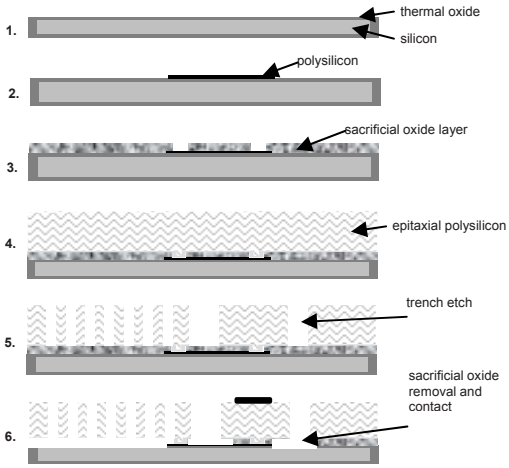

Fig. 1. Schematic illustration of the Thelma surface micro-machining process

The process phases above described concern the most important part of the fabrication process, the one that allows the shaping of single devices on a silicon wafer where hundreds of devices are patterned. In order to obtain the final product, the patterned wafer is bonded with another one, on top of which a simpler patterning has been created which allows for the creation of caps for each of the devices. The couple of wafers bonded together is then ready to be cut in order to single out the devices. The singled MEMS are then wire-bonded with an integrated circuit; the production process is terminated with the molding phase which consists in covering the MEMS + IC with a polymer, leaving outside small electric contacts for the external connection of the MEMS.

Micro-machining processes have an high influence on the properties of materials that are finally obtained, on the surface morphology and on the design possibilities. For a given process, the technological constraints on geometric dimensions and on material properties can be very severe: they force the designer to optimize shapes and mechanical configurations and require research work in order to accurately predict the material and structural behavior also in the possible non-linear regimes.

3. A uniaxial resonant micro accelerometer from a mechanical perspective

Micro-accelerometers, i.e. micro-devices designed to measure external acceleration components, are among the most diffused inertial MEMS. The schematic behavior of a uniaxial accelerometer is represented in Fig. 2.

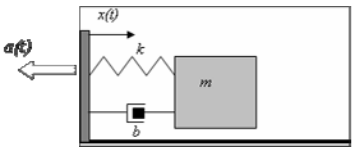

Fig. 2. Schematic representation of a uniaxial accelerometer

In Fig. 2 the rectangular box represents the MEMS which can be connected to any device like e.g. a mobile phone, a lap-top or an air-bag deployer in a car. A mass m, placed inside the box, is constrained by means of some elastic suspension system with overall stiffness k and can move in one direction (horizontal direction x in the figure). Due to the interaction of the moving mass with the surrounding gaseous fluid, and to other dissipative effects, damping influences the mass dynamics and a dashpot with coefficient b represents the overall damping behavior of the device (see Sect. 4). When the MEMS box is subject to a horizontal external acceleration a, the mass moves with respect to the box in the direction opposed to the external acceleration due to the action of inertia forces. The equation of motion of the mass m considered as a 1 d.o.f. oscillator can therefore be written as

$$m\ddot{x} + b\dot{x} + kx = ma \ . \tag{1}$$

In the majority of applications, it can be assumed that the frequency of variation of the external acceleration a is much lower than the eigen-frequency of the undamped oscillator; in these cases by neglecting dynamical terms, a simple relation can be derived which links the external acceleration a to the displacement x of the mass with respect to the MEMS box

$$a \cong (k/m)x \ . \tag{2}$$

Relation (2) allows to obtain the external acceleration a starting from the measurement of the relative displacement x inside the MEMS box. Depending on the physical principle used to measure the displacement x, it is possible to obtain a variety of devices. The most diffused ones are the capacitive accelerometers (see e.g. [6]) in which use is made of capacitive measures, as schematically shown in Fig. 3, where x is derived from the variation of the capacitance of a suitably designed electric circuit.

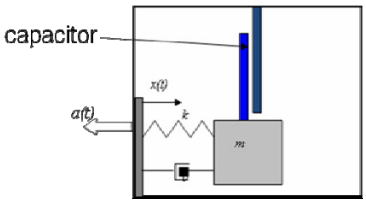

Fig. 3. Schematic representation of a uniaxial capacitive accelerometer

An interesting alternative to capacitive accelerometers is represented by the so-called resonant accelerometers (see e.g. [7–10]). In these devices the link between the external acceleration and the movement of the mass m inside the MEMS box is not given by the displacement x, it is obtained indirectly by the change of frequency of another part of the sensor, kept vibrating at its resonant frequency. This last part, the resonator, can be a flexible beam which is linked to the MEMS box and to the movable mass in such a way that when the mass feels inertia forces due to the external acceleration, the resonating beam is subject to a variation of its axial force and therefore, due to geometric effects, its eigen-frequency can change. A schematic representation of this working principle is given in Fig. 4, where the resonating part is depicted in red.

In [11] it was proposed a new scheme for a resonant accelerometer based on the geometry shown in Fig. 5. The device was also presented in [12] and described in details, together with the electronic control circuit in [10]. Two patents are pending on the device [13, 14].

In the device of Fig. 5, the resonating beams are kept in resonance by means of an electrostatic actuation which is realized through the driving electrode shown in yellow in the figure. The frequency of

vibration of the resonators is continuously measured through an oscillating electronic circuit, not shown in the figure, which senses the resonator response through the sensing electrode (in green in the figure) while keeping the correct signal at the driving electrode.

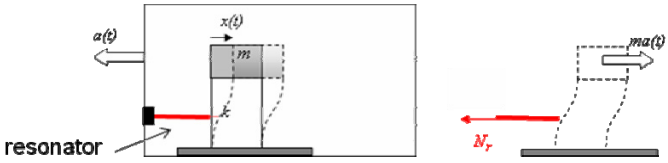

Fig. 4. Schematic representation of a uniaxial resonant accelerometer

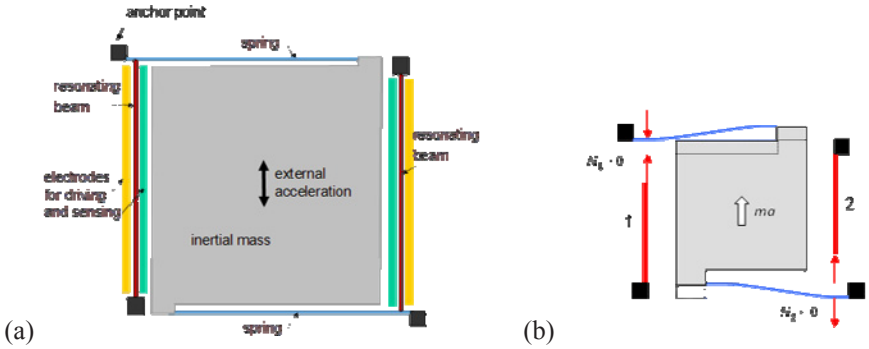

Fig. 5. Uniaxial resonant accelerometer proposed in [11, 12]. (a) General scheme; (b) Mass *m* subject to inertia forces and axial forces in the resonating beams

Figure 5b schematically shows the effect of the external acceleration: when the inertia force causes the movement of mass *m*, the two resonating beams are subject to an axial force, tensile and compressive for beams 1 and 2 respectively. The axial force, in turn, causes a frequency change in the two resonators, increasing the frequency of beam 1 and decreasing that of beam 2. This double frequency change allows to obtain a device with a sensitivity higher than that given by devices of comparable size. In Fig. 6, taken from [10], the differential frequency variation measured on the fabricated devices is shown as a function of external acceleration, measured in *g*, being *g* the gravity acceleration.

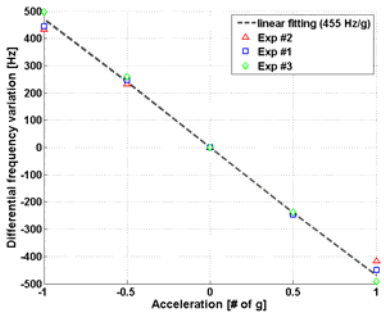

Fig. 6. Variation of the peak frequency difference between the resonators Δf- Δf_0 as a function of the external acceleration in the range of $\pm 1g$. Δf_0 corresponds to the peak frequency difference at $0g$, from [10].

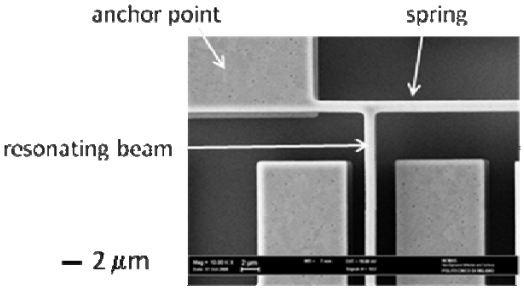

Fig. 7. Detail of the upper left corner of the fabricated uniaxial resonant accelerometer proposed in [11, 12].

Figure 7 shows a detail of the fabricated resonant accelerometer, the upper left corner, where the resonating beam connects to the elastic suspension spring. The Figure shows the typical dimensions of distances of separation between surfaces (the gaps) which are in the order of few microns. Another interesting feature which can be observed from the figure is the slenderness of the resonating beam and of the suspension spring. This feature requires the study of nonlinear effects of both geometric and electrical nature [15]. The position of the resonator with respect to the anchor point has been designed by optimizing the accelerometer sensitivity for given dimensions of the proof mass.

From the above very brief description of a uniaxial resonant accelerometer, some meaningful facts can be recognized which help in defining the role of mechanics in the study, design, fabrication and use of microsystems. These are commented here below, anticipating the contents of subsequent Sects.4–7.

The chosen configurations and shape of the mechanical parts are highly constrained by the fabrication process (see Sect. 2). The final design solutions are an optimal compromise between process constraints, mechanical and electrical responses and reliability issues.

Due to very small dimensions, to the related difficulties of extracting detailed experimental information and to the cost of the production process, modelling and simulation tools are an important ingredient in the study and design of every microsystem. Dedicated products are now available on the market and innovative simulation procedures are continuously being formulated, in particular for the solution of multi-physics and multi-scale problems in MEMS and for the device optimization.

The design goals for a device like the one here briefly described usually are: small dimensions, high sensitivity, low power consumption. These are often contrasting goals, e.g. higher sensitivity obtained increasing the dimensions of the movable mass is in contrast with the necessity to reduce overall dimensions.

The mechanical design of the device must take into careful consideration the non-linear dynamics of the resonating beams, also influenced by the electrostatic forces exerted by the driving and sensing electrodes used to actuate the vibration and to read the displacement of the vibrating beam.

Due to the necessity to accurately measure the eigen-frequency of the resonators, and in some cases to keep this frequency constant in time, every dissipative mechanism related to the resonator response must accurately be considered; these are briefly discussed in Sect. 4 of this paper.

Microsystems analyses typically require coupled multi-physics simulations. The device here discussed clearly shows that the study of the microsystems can be afforded only through a correct consideration of at least the electro-mechanical coupling which governs the resonator behavior. Other kind of coupling can be found e.g. in the gaseous fluid-structure interaction governing the resonator dynamics, in possible electro-magnetic interferences, in the influence of thermal process on the mechanical response.

As far as microsystem reliability is concerned, it is easy to recognize that, being the device built with typical structural parts like slender beams and plates, during the design phase attention must be paid to

mechanical properties. Moreover, due to the fact that the resonating beam vibrate at high frequency, fatigue issues must be carefully checked. As in every structural mechanics problem, the mechanical characterization of materials is extremely important in order to accurately forecast the correct behavior of the designed devices. This issue is discussed in Sect. 5.

Additional reliability problems can come from external loading exceeding the design ranges. As a typical problem, impacts due to accidental drop of the device carrying the micro-accelerometer could be the cause of sudden ruptures and therefore a study on the device limits in the presence of accidental drop impacts is of paramount importance, as discussed in Sect. 6.

Figure 7 allows to appreciate the narrow distances between surfaces which could come into contact during the device use. Permanent adhesion between the surfaces could be then observed due to the presence of forces like capillarity attraction which are difficult to eliminate and van der Waals dispersive forces which cannot be eliminated at all. This clarifies the importance of the study of spontaneous adhesion phenomena as done in Sect. 7.

4. Damping of vibrating parts

Many microsystems contain movable parts which are kept vibrating around their resonance frequency. In the example of Sect. 3 the resonating part is a beam which can change its eigen-frequency due to the action of the external acceleration. In more complex devices like Coriolis-based gyroscopes (see e.g. [16, 17]), a part must vibrate at a given driving velocity in order to cause a Coriolis apparent force acting in a direction orthogonal to its movement and to the rotation axis; in resonators, used e.g. in watches or computers, a vibrating mass must be kept vibrating at a constant frequency with extremely high precision.

The dynamic response of these devices and their energy consumption crucially depend on the damping of the resonating parts.

Damping evaluation, and more generally the evaluation of every dissipative effect, is a difficult task also at the macro scale. In structural dynamics it represents one of the most uncertain ingredients of every dynamic model; in many cases a viscous damping model is used with damping coefficients which are partially unknown or roughly estimated.

In the case of microsystems, a rough estimation of damping could be the source of errors in the design phase and the final device could be useless. The brief introduction here given is based on the hypothesis that the vibrating microsystem has an overall elastic response. In other terms, plasticity, fracture and fatigue are not considered in this discussion.

Damping in microsystems is usually evaluated starting from the quality factor Q, defined as follows in the case of a 1 d.o.f. oscillator.

$$\frac{1}{Q} = 2\pi \frac{\text{total energy lost per cycle}}{\text{stored vibration energy}} = \sum_i 1/Q_i \ , \tag{3}$$

where Q_i represents the quality factor related to the i-th energy dissipation mechanism. Q is therefore inversely proportional to the dissipated energy and it increases when the dissipation sources diminish.

Any reduction of the kinetic vibration energy related to the high frequency vibration of resonating parts is here considered lost for the working regime of the microsystem and therefore is dissipated. This means that the kinetic vibration energy is transformed in other forms of energy, all these energy transformations must be considered as dissipative phenomena in the present context.

One of the main sources of dissipation is represented by the interaction between movable parts inside the MEMS box and the gaseous fluid contained inside it. In this case the fluid-structure interaction is the cause of the main damping mechanism, in the microsystem literature this is simply referred to as fluid

damping (see e.g. [18–20]).

Depending on the device, the volume inside the MEMS box is filled of gas at various pressure levels. As an example, in the case of a gyroscope the pressure is kept at a very low level in order to reduce the fluid damping and consequently reduce the power necessary to keep the resonating part in movement.

At varying pressure levels, the quality factor varies, increasing at decreasing pressure, as qualitatively shown in Fig. 8 where a typical logarithmic scale plot of Q versus pressure is shown.

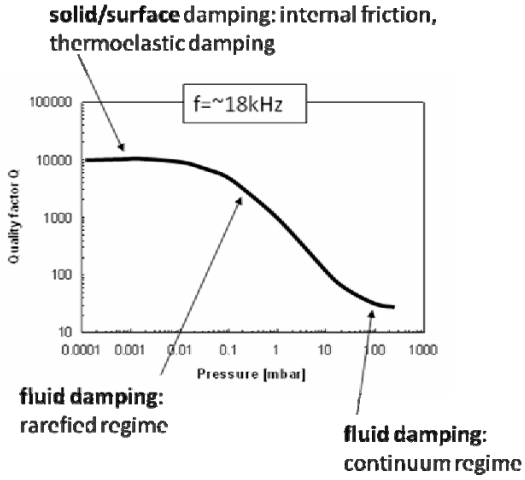

Fig. 8. Quality factor as a function of pressure in microsystems

From Fig. 8 various dissipative regimes can be defined. When the pressure p is very low ($p < 0.01$ mbar), the quality factor does not depend on the pressure level and can be very high but nevertheless limited. This means that fluid damping does not occur for these pressure levels and that other dissipative phenomena occur: this regime is called solid damping in contrast with the fluid damping one. When the pressure is at intermediate levels ($0.01 < p < 10$ mbar), fluid damping prevails on solid damping; in this regime the gas molecules are rarefied and the fluid can not be considered as a continuum. In this case Navier–Stokes equations do not hold and rarefied gas dynamics must be assumed as the correct model. For higher pressures ($p > 10$ mbar), the Navier–Stokes equations can be applied for the study of fluid-structure interaction in microsytems.

Referring in more details to fluid damping, it can be observed that it must be studied and modeled with different strategies depending on the degree of rarefaction of molecules which is correctly represented by the Knudsen number, defined as

$$K_n = \frac{\lambda}{L}, \tag{4}$$

where is the mean free path of molecules and L is a characteristic length scale. At increasing Knudsen number, the gas is more and more rarefied; a possible subdivision in various regimes is given by the following relations:

$$
\begin{aligned}
&K_n \le 10^{-3}, && \text{Navier Stokes no slip bc,}\\
&10^{-3} \le K_n \le 10^{-1}, && \text{Navier Stokes slip bc,}\\
&10^{-1} \le K_n \le 10, && \text{Transition regime,}\\
&K_n > 10, && \text{Free molecular flow.}
\end{aligned}
\tag{5}
$$

In the first case ($K_n < 10^{-3}$), standard Navier–Stokes equations can be used in order to model the fluid, no particular boundary conditions are requested; in the second case ($10^{-3} < K_n < 10^{-1}$), Navier–Stokes equations can still be used, provided that special boundary conditions are considered; the third case ($10^{-1} < K_n < 10$), defines the so called transition regime, while the last one ($K_n > 10$), is the free molecular flow regime.

Various approaches have been proposed in the literature to solve the difficult problem of numerically evaluate fluid damping in microsystems at different pressure levels. Recent examples of numerical approaches able to solve the fluid damping problem at varying pressure can be found in [21] for the second regime, in [22] for the transition regime and in [23, 24] for the free molecular flow regime. The most difficult regime appears to be the transition one, this is why a possible simplification consists in making use of bridging techniques which evaluate the response for free molecular flow and Stokes regimes and build simple interpolation formulae for the intermediate or transition regime, as schematically shown in Fig. 9.

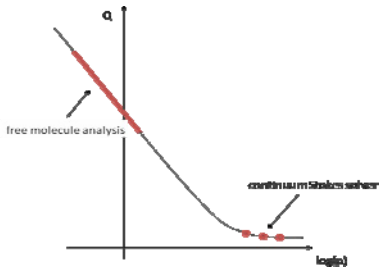

Fig. 9. Schematic representation of bridging techniques for fluid damping evaluation

The full understanding of solid damping mechanisms in microsystems is still an extremely difficult task. A general, schematic, vision is given in Fig. 10, where various solid damping mechanisms are mentioned (see e.g. [19, 25, 26]); notice that among the various sources of damping also unknown sources are mentioned, in order to underline the fact that the understanding of the whole solid damping phenomenology is still partial.

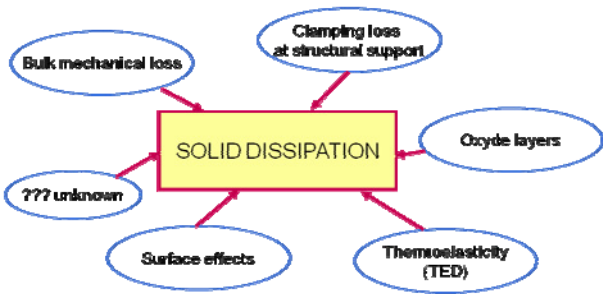

Fig. 10. Schematic representation of possible solid damping mechanisms in MEMS

From the definition of the quality factor (3) and taking into consideration the various solid damping mechanisms referred to in Fig. 10, the total quality factor due to solid damping can be obtained from the following equation.

$$\frac{1}{Q_{\text{sd}}} = \frac{1}{Q_{\text{bulk}}} + \frac{1}{Q_{\text{support}}} + \frac{1}{Q_{\text{oxide}}} + \frac{1}{Q_{\text{TED}}} + \frac{1}{Q_{\text{surface}}} + \frac{1}{Q_{\text{unknown}}}. \tag{6}$$

It can be remarked that, in view of Eq. (6), the quality factor will be less than the smaller of the partial quality factors due to the various mechanisms, i.e.

$$Q \le \min_i \left(Q_i\right). \tag{7}$$

The main source of solid dissipation is the thermo elastic damping (TED) (see e.g. [27, 28]) which manifest at high rate of deformation as in the resonating parts of microsystems. In the case of flexible beams resonating in bending mode, a well known reference solution is the Zener's one [29, 30], derived in the 30s with reference to macro-scale beams. An example of quality factor due to TED with reference to a cantilever micro-beam vibrating in its first bending mode is given in Fig. 11. The plot gives the quality factor due to TED as a function of the ratio of the beam frequency f over the so called transition frequency f_0 (see [31]) defined as

$$f_0 = \frac{\pi}{2} \frac{K_{\text{T}}}{C_p \, \rho} \frac{1}{h^2}, \tag{8}$$

where K_{T} is the thermal conductivity, C_p is the specific heat (at constant pressure), is the mass density, h is the beam thickness.

The line corresponding to QTED theory represents the Zener's solution, the finite element (FE) simulation results have appeared in [31], while the experimental results have been published in [26].

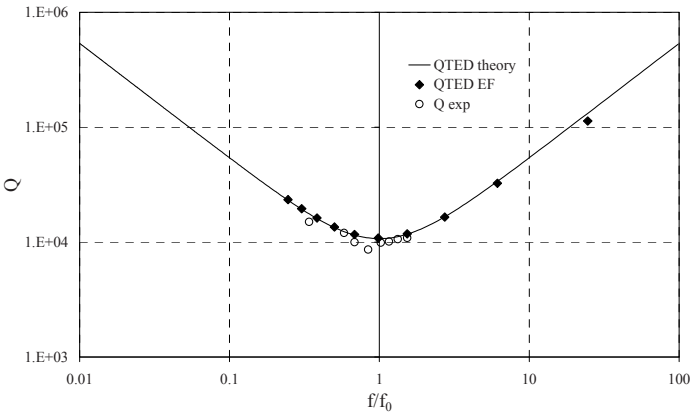

Fig. 11. Quality factor as a function of normalized frequency for an oscillating cantilever micro-beam subject to thermoelastic damping [31]; experimental data from [26].

An alternative representation of the quality factor for the same example is given in Fig. 12 where Q is plotted as a function of the beam length.

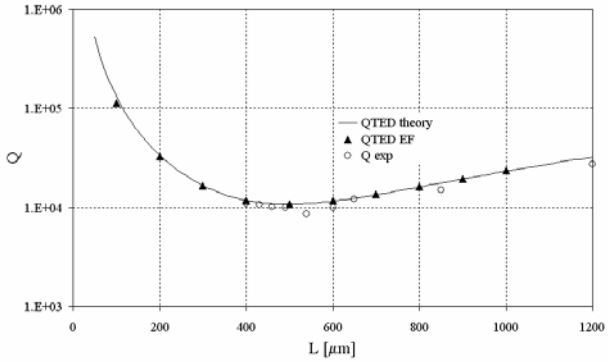

Fig. 12. Quality factor as a function of beam lenght for an oscillating cantilever micro-beam subject to thermoelastic damping [31]; experimental data from [26].

The solution shown in Fig. 11 put in evidence the role of f_0 as a transition frequency. For $f < f_0$ the solid is always in thermal equilibrium and it is possible to speak of an isothermal regime; when $f > f_0$ the system has no time to thermally relax and the regime is adiabatic.

Many experimental results have shown that the quality factor forecast by thermoelasticity (the so-called thermoelastic limit) is not fully attained; in other words, the experimental values of Q which can be found in vibrating micro-beams can be less than the quality factor given by TED. This was shown e.g. in [19, 26] and usually happens for $f < f_0$ at reducing beam dimensions. The possible explanation of this discrepancy must be looked for in the many additional dissipative mechanisms, as depicted in Fig. 10.

Surface effects and surface oxide layers combine the possible influence of different behaviours of surface layers in microbeams and the fact that at decreasing overall dimensions the surface phenomena increase their importance. Different surface treatments have shown that solid damping can change by simply modifying the surface properties. For small size resonators and vacuum measurements, surface losses can dominate.

Bulk mechanical losses [19] include possible internal dissipative mechanisms like internal friction and, in the case of polycrystals, possible internal dissipation associated with interfacial motion and grain boundaries.

Clamping losses is the term used to define the phenomenon of radiation of elastic waves in the structural support of the vibrating beam [26]. In this case the kinetic vibrating energy of the resonating part is partially transformed in another mechanical energy, linked to wave propagation. The problem of estimating the amount of energy lost due to this dissipative mechanism can be tackled with simplified formulations or with fully 3D FE simulation as recently done in [32].

As it can be appreciated from the above introduction to dissipative mechanisms in microsystems, the subject concern many aspects of materials science, materials mechanics and modelling and simulation techniques. Only with a wise merge of many complicate ingredients and with a careful selection of the main dissipative mechanisms related to MEMS behaviour, realistic estimates can be found which could really help in microsystem design and reliability assessment.

5. Mechanical characterization of materials at the micro scale

In Sect. 3 it has been put in evidence the importance of microsystems mechanical reliability. The large scale industrial production obliges producers to more carefully focus on reliability issues related to various causes of failures and in particular on mechanical failures such as fatigue and fracture induced e.g.

by accidental drop (see Sect. 6). It is therefore of paramount importance to measure and control the mechanical properties of materials used in MEMS [33], in primis of polysilicon, which is by far the most diffused material in the production of MEMS.

There exist today many different microscale mechanical test techniques for polysilicon at the micro scale, researchers have explored a variety of physical principles and experimental set-up (e.g. [5, 33–58]). A major distinction can be done between so called off-chip (e.g. [37, 39, 41, 42, 44, 49, 50, 51]) and on-chip (e.g. [5, 35, 38, 40, 43, 46]) methodologies. In both cases the micro-device is generally produced by deposition and etching procedures, as briefly described in Sect. 2. An off-chip tensile test generally resorts to some sort of external gripping mechanism actuating the force together with an external sensor which measures the response of the specimen. On the contrary, on-chip test devices are real MEMS in which actuation and sensing is performed with the same working principles of MEMS.

The on-chip approach for the mechanical characterization of thin and thick polysilicon layers has been pursued recently by the authors ([5, 59–63]), it is briefly discussed in this section starting from a specific example.

The basic idea of the on-chip approach is that the specimen is co-fabricated with the actuator. Therefore an integrated microsystem is created which contains the loading system, the specimen and, typically, the displacement sensor. Electrostatic actuators and displacement sensors are used in most cases. During the tests an input voltage V is applied to the actuator system and a capacitance variation C is measured. The capacitance variation can be related to some meaningful displacement (or rotation) of the specimen through simplified analytical formulae or through electrostatic finite element simulations of the complete device. The corresponding electrostatic force can then be determined as a function of the displacement from the derivative of the electrostatic energy, which, in turn, is proportional to the derivative of the capacitance. This general scheme for data reduction can be applied to many on-chip test structure.

The device here presented was designed to perform both quasi-static and fatigue tests up to complete rupture; it is based on a high number of comb finger electrostatic actuators which load a notched specimen by means of a lever system. It was first published in [61] and then, coupled with electronic control circuits, applied to fatigue testing in [62] and to the assessment of fracture toughness in [63].

In Fig. 13 the detail of the device concerning the loaded specimen is shown by means of an image obtained with a FE simulation and of a SEM image of the fabricated device. The device consists in a lever system that causes a stress concentration in a localized region. The specimen can be divided into four parts: a beam that is the physical link between the frame and the specimen; the lever, that transforms the axial action coming from the beam into a bending moment acting in the notched zone; a notch, that is the most stressed part, where the crack nucleates; and a part fixed to the substrate.

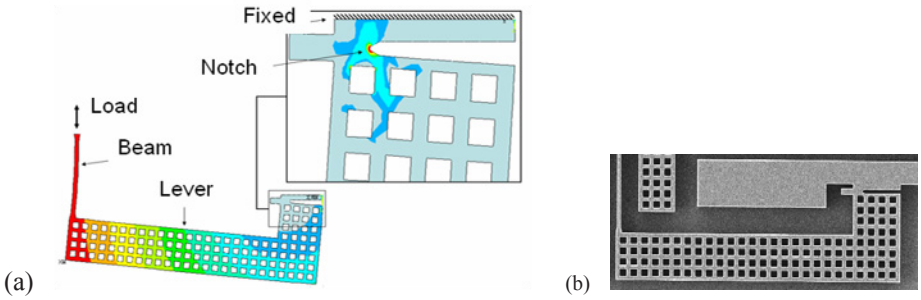

Fig. 13. FE model of the fracture-fatigue test device (a) and SEM image of the realized device (b) [61–63].

The device for on-chip testing here described can be used to perform different kind of mechanical tests, more precisely: monotonic tests in the elastic regime, monotonic tests up to rupture, cycling tests for fatigue assessment, fatigue tests for the creation of pre-cracked notches and subsequent evaluation of fracture toughness trough loading up to complete rupture. Figure 14 shows the notched part of the specimen after complete rupture.

(a) 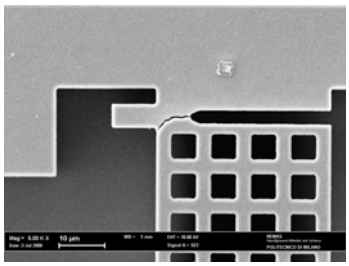 (b) 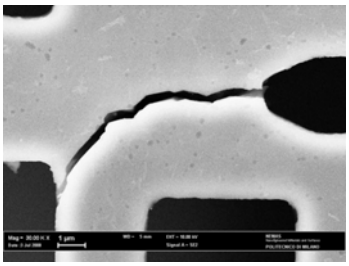

Fig. 14. Detail of the fracture-fatigue test device (a) and zoom on the propagated crack (b) [61–63].

The device was first used to characterize the mechanical behavior of the material in terms of elastic stiffness and nominal values of rupture by means of monotonic loading. As described in more details in [61], an equivalent elastic modulus with a mean value of 143 GPa and a standard deviation of ± 3 GPa was found after testing 31 structures, deposited on the same wafer. The data concerning the rupture of the specimens were interpreted in the framework of the Weibull statistics, widely used in order to assess the mechanical strength of materials in industrial environments (see [59] for a discussion on its application in the framework of on-chip testing methodologies and [64] for the original Weibull formulation). The Weibull modulus was found equal to $m = 25.76$, while the Weibull stress was $_0 = 3.62$ GPa. The Weibull stress represents the level of stress that gives the 63.2% of failure probability for a pure tension specimen with the same size as the reference volume.

As a second application of the on-chip test device, fatigue testing on various devices were performed. A dedicated test set up with a suitably designed electronic circuit was prepared and interesting results concerning the fatigue behaviour of polysilicon were found and published in [62, 63]. Interesting enough, a brittle material like polysilicon shows a clear fatigue response with decreasing nominal strength at increasing number of cycles. As an example, a reduction of the nominal resistance up to 50% was found for a number of cycles in the order of 10^9. The found results were compared with other in the recent literature [42, 43, 46, 48, 52, 53, 55].

The third possible use of the designed test device was the measurement of fracture toughness of polysilicon through on-chip testing. Other proposals in the literature have recently appeared [34, 40, 55]. The basic idea of the proposed methodology was to recreate a crack at the notch tip and, by means of a combination of numerical FE simulations and experimental results, to measure the critical stress intensity factor (Critical SIF). The application of the proposed approach gave a Critical SIF in the range $K_{Ic} = 1.31 – 1.43$ MPa(m)$^{1/2}$. This result gives an idea of the high brittleness of polysilicon materials used in MEMS and therefore of the importance of assessment of mechanical reliability in the various loading conditions that the microsystem will have to sustain during its life.

6. Response to accidental impacts

MEMS are often exposed to accidental shocks or drops during service, especially when mounted on portable devices [65–71]. As for the mechanics of MEMS subject to accidental drops, experimental and

numerical works have to deal with the several length-scales involved in the failure process, ranging from millimeters down to nanometers.

Industrially, the severity of a shock is sometimes defined in terms of the maximum acceleration felt by the sensor. This is in contrast with the results provided, e.g. in [72], where it was shown that the maximum acceleration criterion does not always furnish reliable predictions of MEMS failure, which is instead linked to the stress state in the movable parts of the sensor, see Fig. 15. Since the response of the mechanical parts of the MEMS depends on the evolution of the post-impact acceleration but also on its own geometry, a one-to-one relationship between the acceleration peaks and the stress field can not be established a-priori.

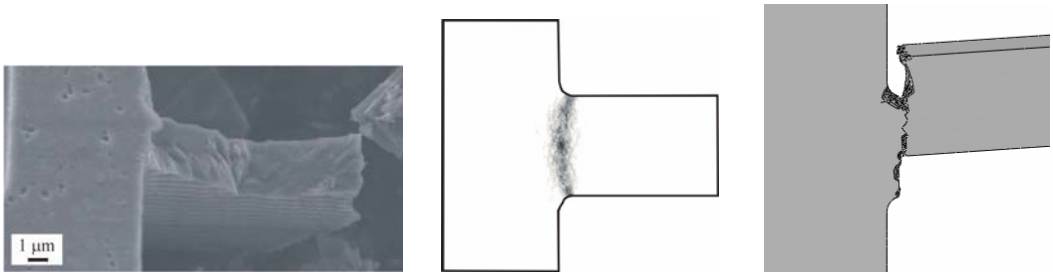

Fig. 15. Shock-induced failure of a uni-axial MEMS accelerometer: (left) experimental evidence [78]; (center) stochastic, three-scale numerical forecast [83]; (right) deterministic, two-scale numerical forecast [83].

A further issue that complicates the matter is the modeling of the input at the MEMS level, allowing for possible filtering effects of the package. For instance, the acceleration experienced by the sensor while bouncing off a massive target body was adopted of a half-sine waveshape in [65, 73, 74] with amplitude and duration of the acceleration pulses assumed a-priori known. This represents an over-simplification of the loading, since complex interactions among stress waves propagating inside the package, sensor dynamics and micro-mechanics driven failure modes turn out to be neglected. In fact, shocks typically cause acceleration peaks exceeding 10^5 g [66], g being the gravity acceleration, but lasting tens or hundreds of ns only. To avoid unexpected failures and enhance the design, if necessary, a reliability analysis of such microsensors is therefore in need of numerical tools able to provide accurate resolutions of the stress/strain fields at the polysilicon film level.

A trivial, homogeneously refined model of these events would be therefore too expensive; a smart way to attack the problem is by resorting to a (decoupled, top-down) multiscale approach. During the last few years, such multiscale framework was developed to attack the problem, see [75–80]. Within this frame, prognostic analyses of shock-induced failures in polysilicon inertial MEMS can account for the main physical processes occurring at all the spanned length-scales. Trying to simplify the approach, three main scales can be singled out: a macroscopic one, wherein the whole package is considered; a mesoscopic one, wherein the movable parts of the sensor are analyzed; a microscopic one, wherein the local failure processes in the polysilicon film are modeled.

As already remarked, the length-scales involved in the shocked-induced response and failure of polysilicon inertial MEMS range from mm (typical size of the sensor package) down to nm (length of the process zone in the cracking polycrystalline silicon film). In case of a drop, at the macro-scale the packaged device is assumed to strike a target body, which is viewed as massive. While bouncing off the target, the device experiences a rigid body-like translational and rotational movement; this motion is characterized by a long time scale (several μs), and can be superseded by much faster phenomena linked to stress waves propagation.

At the mesoscale, MEMS vibrations are induced by displacements of the MEMS anchor(s), and are damped by its interaction with the surrounding fluid (see Sect. 4). The aim of analyses at this scale is to link impact features to possible failure events, assumed to occur where the maximum principal tensile stress in the polysilicon film reaches a critical threshold.

At the microscale the dissipative mechanisms, consisting in the nucleation and propagation of inter- and trans-granular cracks in the brittle polysilicon film, are investigated in details through a cohesive approach, see Fig. 16. A crack is therefore assumed not to abruptly show up, but instead to progressively form and grow due to strength reduction in the process zone region(s). Since analyses have to account for the actual morphology of the polycrystalline film, or for an appropriate representation of it, the hypothesis of homogeneous bodies does not hold true at this scale.

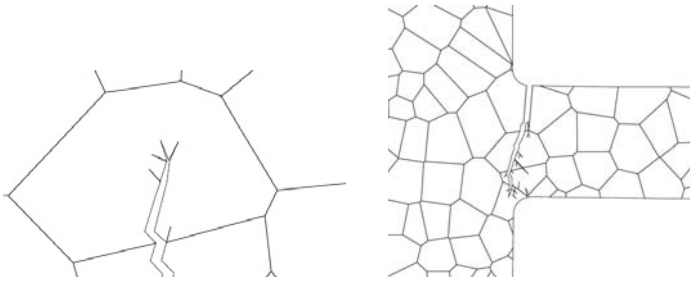

Fig. 16. Exemplary forecast of cracking events at the microscopic (polysilicon) length-scale, adapted from [80]: (left) branching of a trans-granular crack; (right) crack pattern at percolation

The above three-scale approach allowed to accurately match the actual failure location and mode in a uni-axial accelerometer, see Fig. 15. Those results were obtained by considering the morphology and mechanical properties of the polysilicon film to be random at the micro-scale, and hence adopting a Monte Carlo methodology. Since this step turns out to be the most time consuming of the multiscale analysis, in [81, 82] we provided a hybrid deterministic-stochastic upscaling scheme to define micro-structurally informed mechanical properties of a virtual homogeneous film, to be adopted at the meso-scale. Anyway, upscaling is still a main issue, since relevant stochastic morphology indicators and anisotropic, crystal lattice-induced properties of silicon both need to be properly accounted for to provide meaningful outcomes. Hence, in [83] simplified analyses were also carried out with a two-scale approach (avoiding the micro-scale Monte Carlo simulations) and compared to the three-scale ones, showing good accuracy in terms of forecasted failure mode, see Fig. 15.

To further reduce the computational burden without affecting much the accuracy of the results, a reduced order modeling approach was developed in [84] by accounting for the main vibration modes involved in the sensor response to shocks. In the case of the uni-axial MEMS accelerometer, the seismic plate was assumed to be rigid, and connected to the anchor point through deformable slender beams. Hence, the system was reduced to two degrees of freedom only, accounting for torsional and flexural deformations of the slender, support beams: the out-of-plane translation of the plate, and the rotation of the plate around the beam axis. Contact conditions of plate corners with the die and cap surfaces were considered too, to limit the plate motions; in the resulting nonlinear regime, the reduced order model allowed to strongly reduce the computing time, with a speedup factor sometimes exceeding 500 on a personal computer, see [85]. Comparison with the experimentally acquired output signals, caused by excitations with peak accelerations in the range 50 –5 500 g, turned out to be encouraging.

An alternative approach, relying on proper orthogonal decomposition [86] is now under study, see [87]. By exploiting the correlation in an ensemble of observations, a set of orthonormal bases for the

discretized system are obtained through purely algebraic methods, like singular value decomposition. This approach will allow to reduce the computational costs in case of samples featuring complicate geometries, independently of the assumptions on the deformation modes of the suspension springs and of the seismic plate.

7. Spontaneous adhesion

The brief description of the fabrication process reported in Sect. 2 and of the uniaxial accelerometer of Sect. 3 has remarked the very narrow gaps that separate surfaces in real Microsystems. Figure 17 shows another example in which narrow gaps between surfaces can be observed, together with different surface morphologies. The discussion concerning possible accidental impacts of Sect. 6 has also underlined the fact that, due the flexibility of elastic parts in microsystems, surfaces can come into contact during the microsystem's life. Contact mechanics is therefore perse very important in the design of microsystems.

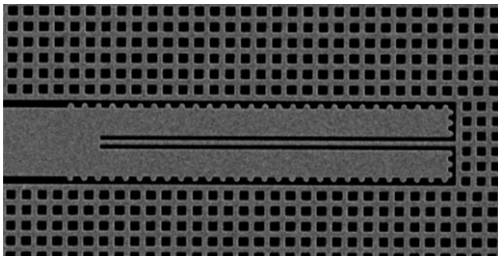

Fig. 17. Detail of a microsystem showing narrow gaps between surface s which could come into contact

Unfortunately, the contact between surfaces can generate another undesirable phenomenon called static friction or stiction which consists in the fact that the surfaces that come into contact can remain attached together thus causing a complete failure of the device. The study of spontaneous adhesion is therefore another mechanical related phenomenon which is of paramount importance for MEMS reliability.

Practically every micro-system contains parts which should maintain the capability of relative motion. In view of the high surface-to-volume ratio of MEMS, the adhesive forces between the parts may exceed the elastic restoring force thus causing the stiction phenomenon. After this catastrophic and irreversible event, the micro-machine could be completely unusable and, consequently, should be replaced.

The stiction phenomenon [88] is strictly correlated with the world of micro-tribology, since friction and wear of contact pairs are tightly connected to the adhesive phenomena on the contacting surfaces (see [89]). A thorough description of the state of the art in nano and micro-tribology can be found, e.g., in the books edited by [90].

Stiction failure can be distinguished in process stiction and in-use stiction. In the first case surfaces remain stuck together at the end of the fabrication process (see Sect. 2), in the second case the phenomenon appears during service operations e.g. due to accidental impacts.

Main sources of spontaneous adhesion are capillary condensation, dispersion forces (van der Waals attractive forces), dielectric charging, hidrogen bonds. The first two being the prevailing ones.

Possible remedies which reduce or avoid the phenomenon are related either to the amount of restoring forces, i.e. the elastic restoring energy of flexible parts which is able to oppose to adhesion energy, or to the kind of surface treatment and morphology. It is clear that increasing the surface roughness will decrease the contact surface and therefore decrease the global adhesion force. Another possibility is to change the surface by adding the deposition of a hydrophobic self assembled monolayer which at least

can almost entirely eliminate the adhesion due to capillary forces.

Studies on stiction failure in MEMs have started in the 90s, mainly related to the experimental investigation of adhesive behavior in micro-systems with the main goal to obtain the adhesive energy. Reference works are in [91–98].

Many efforts have been also devoted to the computational prediction of adhesion. The classical tribological models (Johnson–Kendall–Roberts JKR [99], Derjaguin–Muller–Toropov, DMT [100] or Maugis–Dugdale, MD [101]) can be used in order to compute the adhesive energy between elastic objects with regular shape (namely, a sphere over a flat).

Besides, it has been shown in [102] Cho & Park, 2004 that the problem of adhesive sphere could be solved in a genuine FE environment, by modelling the elastic parts through conventional finite elements and performing a contact analysis. More recently, the Lennard–Jones interatomic potential has been used in FE analysis in order to obtain an innovative formulation of frictionless contact problems [103]. The stochastic nature of the actual rough surface has been considered in many papers, most of which [104] are based on simplified models of elastic-plastic deformation (e.g. Greenwood-Williamson model [105] and its modifications by Chang–Etsion–Bogy etc. [106]). In [107] a simpler model has been adopted, in the sense that rigid-plastic behavior of asperities has been considered and that adhesive forces have been estimated on the basis of the average surface separation. More recently, in [108] the Authors have introduced the adhesive behavior for predicting the wear degradation of electrical contacts at the nano-scale.

Recently in [109–112], the research group proposed a numerical multi-scale approach for the study of spontaneous adhesion phenomena in MEMS. The main ingredient of the numerical approach being the model formulated at the micro-scale, which is based on the following ingredients.

A representative portion of the adhered surfaces is first defined, which dimensions depend on the nature of surfaces, typically a 2 μm × 2 μm reference surface is considered.

Algorithms for the numerical generation of rough surfaces are used to generate surfaces which have the correct statistical properties (see example in Fig. 18). These are obtained considering the height with respect to the average surface as a stochastic process with a given probability density function (p.d.f.).

A 3D FE model of two portions of rough surfaces which undergo a process of adhesion is generated, as shown in Fig. 19.

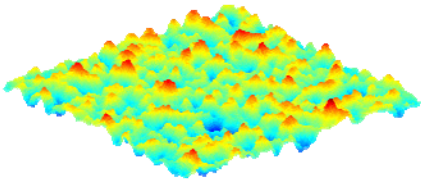

Fig. 18. Example of numerically generated rough surface [109–112]

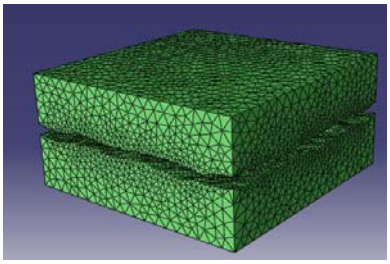

Fig. 19. 3D FE model of portions of rough surfaces [109–112]

Simplified models for the attractive forces which cause adhesion are inserted in the FE model. In particular simplified descriptions of capillary and van der Waals attractive forces are introduced.

A non linear, elasto-plastic behavior is attributed to the solid part of the FE model in order to take into account possible irreversible deformations of asperities in contact cycles.

The proposed computational procedure has been first tested with reference to the classical sphere-over-flat problem in [109–111], and subsequently used in [112] to study the dependence of adhesive energy on humidity, roughness and morphology of surfaces. The obtained results have been successfully compared to experimental tests performed by [113].

A typical value of adhesion energy (i.e. energy per unit surface) obtained with a surface having 15 nm r.m.s roughness, at 60% of Relative Humidity, without taking into consideration the effect of irreversible deformation of asperities, is 10 J/m^2.

8. Closing remarks

This paper presented an overview of mechanical issues related to the design and reliability of Microsystems. An example of a resonant uniaxial accelerometer was used in order to highlight various mechanical problems related to MEMS Engineering. Particular focus has then been given to dissipative phenomena, to the mechanical characterization of materials at the micro scale, to the consequences of accidental drop impacts and to spontaneous adhesion or stiction.

Many other mechanical related issues are of great importance in the MEMS world; among them are quoted here: the whole set of microfluidic problems for liquid fluids and the relevant fluid-structure interaction; the study of wafer-wafer bonding processes were a thermo-compression of thin metal layers, e.g. gold, transforms locally the metal granulometry and create the permanent bonding; the study of the final molding process which involves high stress levels while the polymer is still in a viscous liquid phase; moisture absorption and its consequences on the mechanical response; harsh environment conditions which can be found e.g. in satellite or in cars.

In general terms many inspiring mechanical problems can be found in real microsystem devices which still deserve in deep research work, and highly stimulating theoretical, experimental and computational mechanical challenges.

Acknowledgements

The Authors would like in particular to acknowledge the contribution of: the MSH Group of STMicroelectronics which contributed with research funds and with the production of Microsystems; Cariplo foundation for the funds related to the 2009 project “Surface interaction in micro and nano device”; the Italian Ministry of University and Research MIUR for the PRIN09 project “Multi-scale modelling of materials and structures”.

Some of the results presented in this paper have been obtained in collaboration with other groups of Politecnico di Milano. Colleagues Giacomo Langfelder, Antonio Longoni and Alessandro Tocchio of the Department of Electronics and Information; Luca Magagnin of the Department of Chemistry, Materials and Chemical Engineering; Aldo Frezzotti, Livio Gibelli and Silvia Lorenzani of the Department of Mathematics are gratefully acknowledged.

References

[1] Senturia SD. *Microsystem design*. Dordrecht: Kluwer Ac. Publ.; 2001.

[2] Gardner JW, Varadan VK, Awadelkarim OO. *Microsensors MEMS and smart devices*. Chichester: Wiley; 2001.

[3] Lyshevski SE. *MEMS and NEMS systems, devices and structures*. New York, London: CRC Press; 2002.

[4] Madou MJ. *Fundamentals of microfabrication* New York, London: CRC Press; 2002.
[5] Corigliano A, De Masi B, Frangi A, Comi C, Villa A, Marchi M. Mechanical characterization of polysilicon through on chip tensile tests. *J. Microelectromechanical Systems* 2004; **13**: 2, 200–219.
[6] Beliveau A, Spencer GT, Thomas KA, Roberson SL. Evaluation of MEMS capacitive accelerometers. *IEEE Design and Test of Computers* 1999; 48–56.
[7] Aikele M, Bauer K, Ficker W, Neubauer F, Prechtel U, Schalk J, et al. Resonant accelerometer with self-test. *Sensors and Actuators A* 2001; **92**: 161–167.
[8] Seshia AA, Palaniapan M, Roessig TA, Howe RT, Gooch RW, Shimert TR, et al. A vacuum packaged surface micromachined resonant accelerometer. *J of Microelectromechanical Systems* 2002; **11**: 784–793.
[9] Pinto D, Mercier D, Kharrat C, Colinet E, Nguyen V, Reig B, et al. A small and high sensitivity resonant accelerometer. *Procedia Chemistry* 2009; **1**: 536–539.
[10] Comi C, Corigliano A, Langfelder G, Longoni A, Tocchio A, Simoni B. A resonant microaccelerometer with high sensitivity operating in an oscillating circuit. *J Microelectromech Syst* 2010; **19**: 1140–1152.
[11] Comi C, Corigliano A, Merassi A, Simoni B. A surface micromachined resonant accelerometer with high resolution. *In: Proceedings 7th Euromech Solid mechanics Conference.* Lisbon Portugal, September 7–11, 2009.
[12] Comi C, Corigliano A, Langfelder G, Longoni A, Tocchio A, Simoni B. A high sensitivity uniaxial resonant accelerometer. *In: Proceedings MEMS2010*, Hong Kong, January 24–28, 2010.
[13] Comi C, Corigliano A, Simoni B. Accelerometro risonante MEMS con migliorate caratteristiche elettriche. *Italian Patent n° TO2009A000687*. Deposited September 7, 2009.
[14] Comi C, Corigliano A, Simoni B. International extension (MEMS resonant accelerometer having improved electrical characteristics). *U.S. Patent n° 12/875000*. Deposited September 2, 2010.
[15] Tocchio A, Comi C, Langfelder G, Corigliano A, Longoni A. Enhancing the linear range of MEMS resonators for sensing applications. *IEEE Sensors Journal* 2011; **11**: 3202–3210.
[16] Roland I, Masson S, Ducloux O, Le Traon O, Bosseboeuf A. GaAs 3-axis Coriolis vibrating micro rate gyro: Concept and preliminary characterization. *Procedia Engineering* 2010; **5**: 1442–1445.
[17] Hu ZX, Gallacher BJ, Burdess JS, Fell CP, Townsend K. A parametrically amplified MEMS rate gyroscope. *Sensors and Actuators A* 2011; **167**: 249–260.
[18] Zhang X, Tang WC. Viscous air damping in laterally driven microresonators. *Sens Mater* 1995; **7**: 415.
[19] Yasumura KY, Stowe DT, Chow EM, Pfafman T, Kenny TW, Stipe BC, et al. Quality factor in micron- and submicron-thick cantilevers. *J Microelectromech Syst* 2000; **9**: 117–125.
[20] Ye W, Wang X, Hemmert W, Freeman D, White J. Air damping in lateral oscillating micro-resonators: a numerical and experimental study. *Journal of MEMS* 2003; **12**: 557–566.
[21] Frangi A, Spinola G, Vigna B. On the evaluation of damping in MEMS in the slip-flow regime. *Int J Numerical Methods in Engineering* 2006; **68**: 1031–1051.
[22] Frangi A, Frezzotti A, Lorenzani S. On the application of the BGK kinetic model to the analysis of gas-structure interactions in MEMS. *Computer & Structures* 2007; **85**: 810–817.
[23] Frangi A, Ghisi A, Coronato L. On a deterministic approach for the evaluation of gas damping in inertial MEMS in the free-molecule regime. *Sensor and Actuators A* 2009; **149**: 21–28.
[24] Frangi A. BEM technique for free-molecule flows in high frequency MEMS resonators. *Engineering Analysis with Boundary Elements* 2009; **33**: 493–498.
[25] Mohanty P, Harrington DA, Ekinci KL, Yang YT, Murphy MJ, Roukes ML. Intrinsic dissipation in high frequency micromechanical resonators. *Phys Rev B* 2002; **66**: 085416/1–15.
[26] Le Foulgoc B, Bourouina T, Le Traon O, Bosseboeuf A, Marty F, Breluzeau C, et al. Highly decoupled single-crystal silicon resonators: an approach for the intrinsic quality factor. *J Micromech Microeng* 2006; **16**: 45–53.
[27] Biot MA. Thermoeleasticity and Irreversible Thermodynamics. *J Appl Phys* 1956; **21**, **3**: 240–253.
[28] Lifshitz R, Roukes ML. Thermoelastic damping in micro- and nanomechanical systems. *Phys Rev B* 2000; **61**: 5600–5609.
[29] Zener C. Internal friction in solids, I. Theory of internal friction in reeds. *Phys Rev* 1937; **52**: 230–235.

[30] Zener C. Internal friction in solids, II. General theory of thermoelastic internal friction. *Phys Rev* 1938.; **53**: 90–99.

[31] Ardito R, Comi C, Corigliano A, Frangi A. Solid damping in micro electro mechanical systems. *Meccanica* 2008; **43**: 419–428.

[32] Frangi A, Bugada A, Martello M, Savadkoohi PT. Validation of PML-based models for the evaluation of anchor dissipation in MEMS resonators. *European Journal of Mechanics* 2013; **37**: 256–265.

[33] Sharpe WN. Mechanical properties of MEMS materials, *The MEMS handbook* New York, London: CRC Press, 2002.

[34] Ballarini R, Mullen RL, Yin Y, Kahn H, Stemmer S, Heuer AH. The fracture toughness of polycristalline silicon microdevices: a first report. *J Materials Research* 1997; **12**, 4: 915–922.

[35] Greek S, Ericson F, Johansson S, Schweitz JA. In situ tensile strength measurement and Weibull analysis of thick film and thin film micromachined polysilicon structures. *Thin Solid Films* 1997; **292**: 247–254.

[36] Oostemberg PM, Senturia SD. M-Test: a test chip for MEMS material property measurement using electrostatically actuated test structures. *J. Microelectromechanical Systems* 1997; **6**: 107–118.

[37] Tsuchiya T, Tabata O, Sakata J, Taga Y. Specimen size effect on tensile strength of surface micromachined polycristalline silicon films. *J Microelectromechanical Systems* 1998; **7**: 1: 106–113.

[38] Chi SP, Wensyang H. A microstructure for in situ determination of residual strain. *J Microelectromechanical Systems* 1999; **8**: 200–207.

[39] Sharpe WN, Turner KT, Edwards RL. Tensile testing of polysilicon. *J Experimental Mechanics* 1999; **39**: 162－170.

[40] Kahn H, Tayebi N, Ballarini R, Mullen RL, Heuer AH. Fracture toughness of polysilicon MEMS devices. *Sensor and Actuators A* 2000; **82**: 274–280.

[41] Kramer T, Paul O. Surface Micromachined ring test structures to determine mechanical properties of compressive thin films. *Sensor and Actuators A* 2000; **92**: 292–298.

[42] Ando T, Shikida M, Sato K. Tensile-mode fatigue testing of silicon films as structural material for MEMS. *Sensor and Actuators A* 2001; **93**: 70－75.

[43] Muhlstein CL, Brown SB, Ritchie RO. High-cycle fatigue and durability of polycrystalline silicon thin films in ambient air. *Sensor and Actuators A* 2001; **94**: 177–188.

[44] Chasiotis I, Knauss WG. A new microtensile tester for the study of MEMS materials with the aid of atomic force microscopy, *Experimental Mechanics* 2002; **42**: 51–57.

[45] Sundarajan S, Bhushan B. Developement of AFM-based techniques to measure mechanical properties of nanoscale structures. *Sensors and Actuators A* 2002; **101**: 338–351.

[46] Kahn H, Ballarini R, Bellante JJ, Heuer AH. Fatigue failure in polysilicon not due to simple stress corrosion cracking. *Science* 2002; **298**: 1215–1218.

[47] Tsuchiya T, Shikida M, Sato K. Tensile testing system for sub-micrometer thick films. *Sensors and Actuators A* 2002; **97-98**: 492–496.

[48] Bagdahn J, Sharpe WN Jr. Fatigue of polycrystalline silicon under long-term cyclic loading. *Sensors and Actuators A* 2003; **103**: 9–15.

[49] Bagdahn J, Sharpe WN Jr, Jadaan O. Fracture strength of polysilicon at stress concentrations. *J Microelectromechanical Systems* 2003; **12**: 302–312.

[50] Chasiotis I, Knauss WG. The mechanical strength of polysilicon films: Part 1. The influence of fabrication governed surface conditions. *J Mech Phys Solids* 2003a; **51**: 1533–1550.

[51] Chasiotis I, Knauss WG. The mechanical strength of polysilicon films: Part 2. Size effects associated with elliptical and circular perforations. *J Mech Phys Solids* 2003b; **51**: 1551–1572.

[52] Kahn H, Ballarini R, Heuer AH. Dynamic fatigue of silicon, Current Opinion in Solid State and Materials. *Science* 2004; **8**: 71–76.

[53] Muhlstein CL, Howe RT, Ritchie RO. Fatigue of polycrystalline silicon for microelectromechanical system applications: crack growth and stability under resonant loading conditions. *Mechanics of Materials* 2004; **36**: 13–33.

[54] Zhu Y, Corigliano A, Espinosa HD. A thermal actuator for nanoscale in-situ microscopic testing: design and characterization. *J Micromechanics and Microengineering* 2006; **16**: 242–253.

[55] Chasiotis I, Cho SW, Jonnalagadda K. Fracture toughness and subcritical crack growth in polycrystalline silicon. *J Applied Mechanics* 2006; **73**: 714–722.

[56] Corigliano A, Domenella L, Espinosa HD, Zhu Y. Electro-thermal actuator for on-chip nanoscale tensile tests: analytical modelling and multi-physics simulations. *Sensor Letters* 2007; **5**: 1–16.

[57] Cho SW, Chasiotis I. Elastic properties and representative volume element of polycrystalline silicon for MEMS. *Experimental mechanics* 2007; **47**: 37–49.

[58] McCarty A, Chasiotis I. Description of brittle failure of non-uniform MEMS geometries. *Thin solid films* 2007; **515**: 3267–3276.

[59] Corigliano A, Cacchione F, De Masi B, Riva C. On-chip electrostatically actuated bending tests for the mechanical characterization of polysilicon at the micro scale. *Meccanica* 2005; **40**: 485–503.

[60] Cacchione F, Corigliano A, De Masi B, Riva C. Out of plane vs. in plane flexural behaviour of thin polysilicon films: mechanical characterization and application of the Weibull approach. *Microelectronics Reliability* 2005; **45**: 1758–1763.

[61] Corigliano A, Cacchione F, Zerbini S. Mechanical characterization of low dimensional structures through on-chip tests. In Yang F, Li JCM editors, *Micro and Nano Mechanical Testing of Materials and Devices*, Springer, 2008; 349–384.

[62] Langfelder G, Longoni A, Zaraga F, Corigliano A, Ghisi A, Merassi A. A new on-chip test structure for real time fatigue analysis in polysilicon MEMS. *Microelectronics Reliability* 2009; **49**: 120–126.

[63] Corigliano A, Ghisi A, Langfelder G, Longoni A, Zaraga F, Merassi A. A microsystem for the fracture characterization of polysilicon at the micro scale. *European J. of Mechanics* 2011; **30**: 127–136.

[64] Weibull W. A statistical distribution of wide applicability. *J Appl Mech* 1951; **18**: 293–297.

[65] Srikar VT, Senturia SD. The reliability of microelectromechanical systems (MEMS) in shock environments. *J of Microelectromechanical Systems* 2002; **11**: 206–214.

[66] Wagner U, Franz J, Schweiker M, Bernhard W, Muller-Friedler R, Michel B, et al. Mechanical reliability of MEMS-structures under shock load. *Microelectronics Reliability* 2001; **41**: 1657–1662.

[67] Li GX, Shemansky FA. Drop test and analysis on micro machined structures. *Sensors and ActuatorsA* 2000; **85**, 280－286.

[68] Ghaffarian R. CCGA packages for space applications. *Microelectronics Reliability* 2006; **46**: 2006–2024.

[69] [69] Varghese J, Dasgupta A. Test methodology for durability estimation of surface mount interconnects under drop testing conditions. *Microelectronics Reliability* 2007; **47**: 93–103.

[70] Luan J, Tee TY, Peck E, Lim CT, Zhong Z. Dynamic responses and solder joint reliability under board level drop test. *Microelectronics Reliability* 2007; **47**: 450–460.

[71] Cheng Z, Huang W, Cai X, Xu B, Luo L, Li X. Packaging effects on the performances of MEMS for high-g accelerometer: frequency domain and time-domain analyses. *In: Proceeding of the Sixth IEEE CPMT Conference on High Density Microsystem Design and Packaging and Component Failure Analysis* (HDP'04), 282－289, Shanghai, China, July 2004.

[72] Suhir E. Is the maximum acceleration an adequate criterion of the dynamic strength of a structural element in an electronic product? *IEEE Transactions on Components, Packaging and Manifacturing Technology* 1997; **20**: 513–517.

[73] Jiang D, Shu D. Predication of peak acceleration of one degree of freedom structures by scaling law. *ASCE Journal of Structural Engineering* 2005; **131**: 582–588.

[74] Hauck T, Li G, McNeill A, Knoll H, Ebert M, Bagdahn J. Drop simulation and stress analysis of MEMS devices. In *Proceedings of the International Conference on Thermal, Mechanical and Multiphysics Simulation and Experiments in Micro-Electronics and Micro-Systems* (EuroSimE 2006), 203–207, Como, Italy, April 2006.

[75] Mariani S, Ghisi A, Corigliano A, Zerbini S. Multi-scale analysis of MEMS sensors subject to drop impacts. *Sensors* 2007; **7**: 1817–1833.

[76] Corigliano A, Cacchione F, Frangi A, Zerbini S. Numerical modelling of impact rupture in polysilicon microsystems. *Computational Mechanics* 2008; **42**: 251–259.

[77] Mariani S, Ghisi A, Fachin F, Cacchione F, Corigliano A, Zerbini S. A three-scale FE approach to reliability analysis of MEMS sensors subject to impacts. *Meccanica* 2008; **43**: 469–483.

[78] Mariani S, Ghisi A, Corigliano A, Zerbini S. Modeling impact-induced failure of polysilicon MEMS: a multi-scale approach. *Sensors* 2009; **9**: 556–567.

[79] Ghisi A, Fachin F, Mariani S, Zerbini S. Multi-scale analysis of polysilicon MEMS sensors subject to accidental drops: Effect of packaging. *Microelectronics Reliability* 2009; **49**: 340–349.

[80] Mariani S, Martini R, Ghisi A, Corigliano A, Simoni B. Monte Carlo simulation of micro-cracking in polysilicon MEMS exposed to shocks. *International Journal of Fracture* 2011; **167**: 83–101.

[81] Mariani S, Martini R, Ghisi A, Corigliano A, Beghi M. Overall elastic properties of polysilicon films: A statistical investigation of the effects of polycrystal morphology. *International Journal for Multiscale Computational Engineering* 2011; **9**: 327–346.

[82] Mariani S, Martini R, Corigliano A, Beghi M. Overall elastic domain of thin polysilicon films. *Computational Materials Science* 2011; **50**: 2993–3004.

[83] Mariani S, Ghisi A, Corigliano A, Martini R, Simoni B. Two-scale simulation of drop-induced failure of polysilicon MEMS sensors. *Sensors* 2011; **11**: 4972–4989.

[84] Ghisi A, Kalicinski S, Mariani S, De Wolf I, Corigliano A. Polysilicon MEMS accelerometers exposed to shocks: numerical-experimental investigation. *J of Micromechanics and Microengineering* 2009; **19**: 035023.

[85] Ghisi A, Mariani S, Corigliano A, Zerbini S. Physically-based reduced order modelling of a uni-axial polysilicon MEMS accelerometer. *Sensors* 2012; **12**: 13985–4003.

[86] Kerschen G, Golinval JC, Vakakis A, Bergman L. The method of proper orthogonal decomposition for dynamical characterization and order reduction of mechanical systems: an overview. *Nonlinear Dynamics* 2005; **41**: 147－169.

[87] Corigliano A, Dossi M, Mariani S. Domain decomposition and model order reduction methods applied to the simulation of multiphysics problems in MEMS. *Computers & Structures* 2013; **122**: 113–127.

[88] Tas NR, Gui C, Elwenspoek M. Static friction in elastic adhesion contacts in MEMS. *J of Adhesion Science and Technology* 2003; **17**: 547–561.

[89] Bhushan B. Nanotribology and nanomechanics of MEMS/NEMS and BioMEMS/BioNEMS materials and devices. *Microelectronic Engineering* 2007; **84**: 387－412.

[90] Bhushan B. *Nanotribology and Nanomechanics*. Berlin: Springer; 2011.

[91] Mastrangelo CH, Hsu CH. Mechanical stability and adhesion of microstructures under capillary forces-Part I: basic theory. *J of Microelectromechanical Systems* 1993; **2**: 33–43.

[92] Mastrangelo CH, Hsu CH. Mechanical stability and adhesion of microstructures under capillary forces-Part II: experiments. *J of Microelectromechanical Systems* 1993; **2**: 44–55.

[93] De Boer MP, Michalske TA. Accurate method for determining adhesion of cantilever beams. *J of Applied Physics* 1999; **86**: 817–827.

[94] Jones EE, Begley MR, Murphy KD. Adhesion of micro-cantilevers subjected to mechanical point loading: Modelling and experiments. *J of the Mechanics and Physics of Solids* 2003; **51**: 1601–1622.

[95] [95] Leseman ZC, Carlson SP, Mackin TJ. Experimental measurements of the strain energy release rate for stiction-failed microcantilevers using a single-cantilever beam peel test. *J of Microelectromechanical Systems* 2007; **16**: 38–43.

[96] Bachmann D, Kühne S, Hierold C. Determination of the adhesion energy of MEMS structures by applying Weibull-type distribution function. *Sensors and Actuators A* 2006; **132**: 407–414.

[97] Yu T, Ranganathan R, Johnson N, Yadav N, Gale R, Dallas T. In situ characterization of induced stiction in a MEMS. *J of Microelectromechanical Systems* 2007; **16**: 355–364.

[98] Basu S, Prabhakar A, Bhattacharya E. Estimation of stiction force from electrical and optical measurements on cantilever beams. *J of Microelectromechanical Systems* 2007; **16**: 1254–1262.

[99] Johnson KL, Kendall K, Roberts AD. Surface energy and the contact of elastic solids. *Proceedings of the Royal Society A* 1971; **324**: 301–313.

[100] Derjaguin BV, Muller VM, Toporov YP. Effect of contact deformations on the adhesion of particles. *J of Colloid and Interface Science* 1975; **53**: 314–326.

[101] Maugis D. Adhesion of spheres: The JKR-DMT transition using a dugdale model. *J of Colloid and Interface Science* 1992; **150**: 243–269.

[102] Cho S, Park S. Finite element modelling of adhesive contact using molecular potential. *Tribology International* 2004; **37**: 763–769.

[103] Sauer RA, Wriggers P. Formulation and analysis of a three-dimensional finite element implementation for adhesive contact at the nanoscale. *Computer Methods in Applied Mechanics and Engineering* 2009; **198**: 3871–3883.

[104] Hariri A, Zu J, Mrad RB. Modelling of wet stiction in microelectromechanical systems (MEMS). *J of Microelectromechanical Systems* 2007; **16**: 1276–1285.

[105] Greenwood JA, Williamson JBP. Contact of nominally flat surfaces. *Proceedings of the Royal Society A* 1966; **295**: 300–319.

[106] Chang WR, Etsion I, Bogy DB. Elastic-plastic model for the contact of rough surfaces. *J of Tribology* 1987; **109**: 257–263.

[107] Van Spengen MW, Puers R, De Wolf I. A physical model to predict stiction in MEMS. *J of Micromechanics and Microengineering* 2002; **12**: 702–713.

[108] Dadgour HF, Hussain MM, Cassell A, Singh N, Banerjee K. Impact of scaling on the performance and reliability degradation of metal-contacts in NEMS devices. *Proceedings IEEE International Reliability Physics Symposium* 2011; 3D.3.1.

[109] Ardito R, Corigliano A, Frangi A. On the analysis of spontaneous adhesion in MEMS. *Proceedings 10th International Conference on Thermal, Mechanical and Multi-Physics Simulation and Experiments in Microelectronics and Microsystems*, EuroSimE 2009.

[110] Ardito R, Corigliano A, Frangi A. Multiscale finite-element models for predicting spontaneous adhesion in MEMS. *Mecanique et Industries* 2010; **11**: 177–182.

[111] Ardito R, Corigliano A, Frangi A. Finite element modelling of adhesion phenomena in MEMS. *In: Proceedings 11th International Conference on Thermal, Mechanical and Multi-Physics Simulation, and Experiments in Microelectronics and Microsystems*, EuroSimE 2010.

[112] Ardito R, Corigliano A, Frangi A. Modelling of spontaneous adhesion phenomena in Micro-Electro-Mechanical Systems 2013; **39**: 144–152.

[113] Delrio FW, De Boer MP, Knapp JA, Reedy Jr., ED, Clews PJ, Dunn ML. The role of van der Waals forces in adhesion of micromachined surfaces. *Nature Materials* 2005; **4**: 629–634.